energies

MDPI

Article

A Comparison of Energy Consumption Prediction Models Based on Neural Networks of a Bioclimatic Building

Hamid R. Khosravani [1,2], María Del Mar Castilla [3,*], Manuel Berenguel [3], Antonio E. Ruano [1,2] and Pedro M. Ferreira [4]

Received: 15 October 2015; Accepted: 12 January 2016; Published: 20 January 2016
Academic Editor: Chi-Ming Lai

1 Faculty of Science and Technology, University of Algarve, Campus Gambelas, Faro, Portugal; hkhosravani@csi.fct.ualg.pt (H.R.K.); aruano@ualg.pt (A.E.R.)
2 Institute of Mechanical Engineering (IDMEC), Instituto Superior Técnico, Universidade de Lisboa, Lisboa, Portugal
3 Department of Computer Science, Automatic Control, Robotics and Mechatronics Research Group, University of Almería, Agrifood Campus of International Excellence (ceiA3), CIESOL, Joint Center University of Almería-CIEMAT, Almería, Spain; beren@ual.es
4 LaSIGE, Faculdade de Ciências, Universidade de Lisboa, Portugal; pmf@ciencias.ulisboa.pt
* Correspondence: mcastilla@ual.es; Tel.: +34-950-21-41-55; Fax: +34-950-01-51-29

Abstract: Energy consumption has been increasing steadily due to globalization and industrialization. Studies have shown that buildings are responsible for the biggest proportion of energy consumption; for example in European Union countries, energy consumption in buildings represents around 40% of the total energy consumption. In order to control energy consumption in buildings, different policies have been proposed, from utilizing bioclimatic architectures to the use of predictive models within control approaches. There are mainly three groups of predictive models including engineering, statistical and artificial intelligence models. Nowadays, artificial intelligence models such as neural networks and support vector machines have also been proposed because of their high potential capabilities of performing accurate nonlinear mappings between inputs and outputs in real environments which are not free of noise. The main objective of this paper is to compare a neural network model which was designed utilizing statistical and analytical methods, with a group of neural network models designed benefiting from a multi objective genetic algorithm. Moreover, the neural network models were compared to a naïve autoregressive baseline model. The models are intended to predict electric power demand at the Solar Energy Research Center (Centro de Investigación en Energía SOLar or CIESOL in Spanish) bioclimatic building located at the University of Almeria, Spain. Experimental results show that the models obtained from the multi objective genetic algorithm (MOGA) perform comparably to the model obtained through a statistical and analytical approach, but they use only 0.8% of data samples and have lower model complexity.

Keywords: predictive model; electric power demand; neural networks; multi objective genetic algorithm (MOGA); data selection

1. Introduction

Due to fast economic development affected by industrialization and globalization, energy consumption has been steadily increasing over the last years [1,2]. Industry, transportation and buildings are the three main economic sectors which consume a significant amount of energy, with buildings accounting for the biggest proportion. For example in European Union countries, energy consumption in buildings represents about 40% of the total energy consumption [3]. In the

USA, more than 44% of domestic energy consumption corresponds to heating, ventilating and air conditioning (HVAC) systems in buildings [4]. Studies have shown that by following the current energy consumption pattern, the world energy consumption may increase more than 50% before 2030 [5], while most of the energy resources are not renewable in nature. Moreover, the usage of energy causes environmental degradation [2]. Therefore, energy consumption management is a very significant problem not only to tackle the losses resulting from increasing consumption patterns but also to improve the performance of building energy systems. With respect to energy management, a variety of policies have been considered. In recent years, there has been a focus on bioclimatic architectures for buildings to reduce the indoor consumption of energy. In this kind of architecture, buildings are designed based on the local climate conditions. These include wind speed and direction, daily exterior temperature and relative humidity, as well as diverse passive solar technologies where heating and cooling techniques passively absorb solar radiation or protect from it without containing mobile elements [6–8]. Besides environmental variables, physical properties of buildings are considered in bioclimatic architectures, such as shape, buildings' orientation related to the sun and wind, wall thickness and roof construction [6,9].

Utilizing renewable energy sources such as biomass, hydropower, geothermal, solar, wind and marine energies have been considered as alternatives for conventional energy resources in most developed and developing countries [10,11]. In the European Union, the renewable energies use share is 20% of the total energy consumption and 10% of renewable energies will be used in transportation by 2020 [12]. Using renewable energies not only helps ensure the security of non-renewable energy supply in future, but also minimizes environmental degradation [11].

Prediction of energy use in buildings has received a remarkable amount of attention from researchers [1,3,13,14], as an approach to reduce energy consumption, which is intended to conserve energy and reduce environmental impacts [3]. The prediction of energy usage in buildings and modelling the behaviour of the corresponding energy system, are complicated tasks due to influential factors such as weather variables, building construction, thermal properties of the physical materials and occupants' activities [3]. Furthermore, there are several nonlinear inter-relationships among the involved variables, often in a noisy environment, which amplify the difficulty in identifying the precise interaction among them [15].

The methods aiming to predict building energy consumption can be categorized mainly into statistical, engineering and artificial intelligence ones. A review on prediction methods can be found in [3,16]. Engineering methods, which are detailed comprehensive methods, use the structural properties of buildings in the form of physical principles and thermal dynamics equations, as well as environmental information such as climate conditions, occupants, their activities and HVAC equipment parameters. On the one hand, these methods need a high level of details about the structural and thermal parameters of buildings that are not always available and, on the other hand, since engineering methods depend on complex physical principles, a high level of expertise is needed to elaborately develop the corresponding models [3,17]. To reduce the complexity of the detailed comprehensive engineering methods, simplified methods have been proposed, which can be seen in [18,19].

Statistical methods use historical data to correlate energy consumption as target with most influential variables as inputs. Hence, the quality and quantity of historical data has a crucial role in developing statistical models [17,20]. Unlike engineering methods, statistical methods provide models with a smaller number of variables and much less physical understanding. Regression models, conditional demand analysis (CDA), auto regressive moving average (ARMA), auto regressive integrated moving average (ARIMA) and Gaussian mixture models (GMM) are some instances of statistical models [20–23].

In recent years, artificial intelligence methods such as neural networks, support vector machines and fuzzy logic have been widely considered in applications of energy consumption. Like statistical methods, artificial intelligence methods use historical data reflecting the behaviour of the process to be modelled. Neural networks have shown a high capability to capture complex nonlinear relationships

between inputs and outputs. Since the energy consumption process has a nonlinear behaviour, neural networks are mostly applied in this domain. In addition, they are quicker and easier to develop than engineering and statistical methods, while being accurate estimators. Some instances of neural network based models may be found in [15,17,24–28].

Recently, support vector machines have received much attention as quick methods to build predictive models in energy consumption applications. They can provide models with a high level of generalization based on a number of data. Applications to the prediction of energy utilization can be viewed, for instance, in [29–31].

Besides neural network- and support vector machine-based models, another kinds of models which benefit from fuzzy logic have been considered. Fuzzy logic deals with imprecise reality and handles the concept of truth value ranging between completely true and completely false (1–0) [32]. Some models of this type can be seen in [33,34].

As mentioned earlier, both statistical and artificial intelligence methods need sufficient historical data to provide accurate models. In cases where limited amounts of data are available and the information about the process to be modelled is partially known, grey models are suitable alternatives to the prediction of time series associated with processes [35–37].

The objective of this paper is to compare a neural network based model obtained in [17] with the models obtained by a multi objective genetic algorithm (MOGA), to predict the electric power demand of the Solar Energy Research Center (Centro de Investigación en Energía SOLar or CIESOL in Spanish) building located at University of Almeria, Spain. The authors in [17] determined the structure and the order of the model by statistical and analytical methods while in this article a non-dominated set of models is generated by a MOGA considering a set of objectives to be optimized. For the sake of completion, the performance of MOGA models is also compared with the results obtained by a naive autoregressive baseline (NAB) approach, introduced in [38].

This paper is organized as follows: in Section 2, the structural properties and power demand profile of the CIESOL building are briefly described. The model proposed in [17] and the models generated by MOGA are widely described in Sections 3 and 4 respectively. Experimental results are shown in Section 5. Finally, some conclusions are drawn in Section 6.

2. Experimental Setup: The Solar Energy Research Center Building

The CIESOL building (Figure 1a), is a mixed solar energy research centre operated between the Centre for Energy, Environment and Technology (in Spanish the Centro de Investigaciones Energéticas, MedioAmbientales y Tecnológicas—CIEMAT) and the University of Almería, situated in the south-east of Spain. This geographical location is characterized by having a typical semi-desertic Mediterranean climate [39]. This building is divided into two floors with a total surface of approximately 1100 m^2. More specifically, the upper floor is composed by four laboratories, the director's office and a meeting-room. On the lower floor, five offices, four laboratories, two bathrooms and a kitchen are located. Besides these, the machinery of the solar cooling installation is placed into an environment which occupies two floors.

This building has been designed and built within a research project named PSE-ARFRISOL [40], following bioclimatic architecture criteria. Therefore, it makes a beneficial use of natural ventilation and solar energy in order to reduce energy consumption and CO_2 emissions. To do that, it employs a HVAC system based on solar cooling, which can be observed in Figure 1b, composed by a solar collector field, a hot water storage system, a boiler and an absorption machine with its refrigeration tower [40], and a photovoltaic (PV) power plant with a peak power of 9 kW which provides electricity to the building (Figure 1c,d). Furthermore, a wide network of sensors has been installed in order to monitor the most representative enclosures of the building. Concretely, this network of sensors includes, among others, air temperature, relative humidity, CO_2 concentration, solar radiation, wind velocity and power consumption sensors. Moreover, these sensors are connected to different Compact FieldPoint modules from National Instruments (Madrid, Spain) that are distributed by means of

an Industrial Ethernet network all around the building [40]. Data provided by the network of sensors are being stored through a supervisory control and data acquisition (SCADA) system developed with LabVIEW® [40]. Finally, it is necessary to take into account that this building is a research centre which includes chemical, environmental analysis, and modelling and control research groups. Hence, the machinery, other electrical devices and experiments performed by these research groups alter the energy use profile of the building in comparison with more common ones, such as residential buildings.

Figure 1. The Solar Energy Research Center (CIESOL or Centro de Investigación en Energía SOLar in Spanish) building: (**a**) exterior of the CIESOL building; (**b**) solar cooling installation; (**c**) photovoltaic (PV) power plant: PV panels; and (**d**) PV power plant: PV inverters.

2.1. Power Demand Profiles of the Solar Energy Research Center Building

From a power demand point of view, the CIESOL building has some special characteristics mainly derived from the research tasks which are being developed inside it. Therefore, it is necessary to perform an exhaustive analysis of the different energy demand profiles which can be found at the CIESOL building. Specifically, a statistical characterisation involving certain parameters like arithmetic mean ($\overline{x}$), standard deviation (σ), and minimum and maximum values of the power demand (minimum and maximum, respectively) under several conditions (different season and types of days), has been performed (Table 1).

Table 1. Statistical analysis of the power demand profiles (in kW).

Condition	$\overline{x}$	σ	Minimum	Maximum
Working day	24.36	6.39	17.39	44.17
Non-working day	19.45	1.83	12.72	23.86
Winter	26.45	4.55	18.93	39.48
Spring	23.91	6.76	12.56	42.79
Autumn	24.23	4.58	15.85	48.14
Summer	28.74	8.67	16.28	63.48

To predict the power demand within a building, it is necessary to consider numerous energy consuming elements, such as illumination, electrical devices, HVAC systems, *etc.* At the CIESOL building, the element which has the greatest energy consumption is the solar cooling installation. Furthermore, to calculate the total energy demand of the CIESOL building it is necessary to consider both the energy supplied by the electricity company and the energy produced by the PV power plant which is directly consumed by the building, that is, at this moment it is not possible to store the energy from the PV power plant.

Firstly, the main differences according to typical power demand profiles between working and non-working days have been studied, as presented in Figure 2. To do that, a typical day for each demand profile, considering working and non-working days, and each season, has been selected as a function of several environmental variables: mean, maximum and minimum temperature, temperature ranges and solar radiation. The methodology consists of selecting the day with the minimum value obtained from the sum of the weighted absolute difference between each parameter (daily) and the mean value of this parameter along the analysed period. A detailed description of the procedure which has been followed can be found in [41]. It can be observed that power demand on a working day begins to increase around 8:00 am and starts to decrease at 5:00 pm, reaching a stationary value around 8:00 pm, whereas, on a non-working one it has a stationary value approximately equal to 20 kW, mainly due to the machinery and experimental tests performed inside this building. From the perspective of the statistical analysis shown in Table 1, it can be inferred that the mean power demand for a working day is equal to 24.36 kW with a standard deviation of 6.39 kW. On the contrary, for a non-working day, a mean power demand of 19.45 kW and a standard deviation equal to 1.83 kW have been obtained. In addition, working days also present a higher peak power demand, in comparison with non-working days.

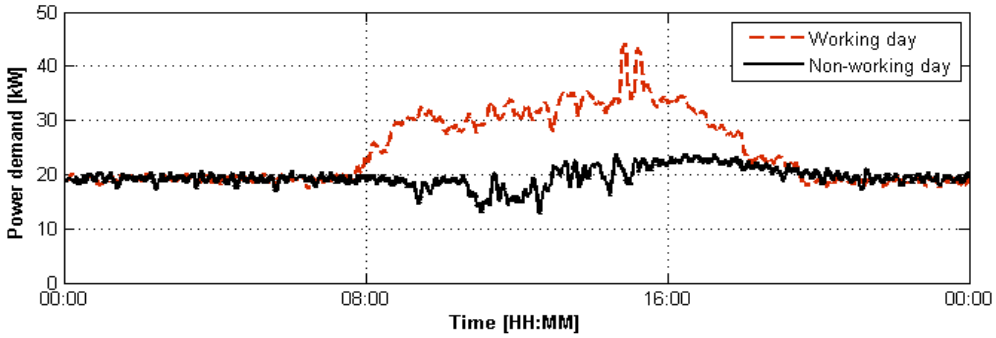

Figure 2. Energy demand profiles for working and non-working days.

Secondly, a detailed examination of the power demand of the CIESOL building through a typical week (from Monday to Sunday), along different environmental conditions has been performed, as shown in Figure 3. The main objectives of this analysis were to determine if there were representative differences among the different seasons of the year and also to identify if there was any characteristic element of the building able to considerably influence its power demand. More specifically, as it can be deduced from Figure 3, the different seasons of the year follow an analogous pattern among working and non-working days. In addition, it can also be inferred that spring and summer seasons present a higher power demand in comparison with winter and autumn. Besides, along the summer season there are several power demand peaks that do not follow any specific pattern associated with the type of day. Therefore, in order to clarify this issue, a detailed analysis of this fact has been performed, and the main conclusions derived from it were that these peaks were associated with the use of a heating pump (for research purposes) and the solar cooling installation. Hence, as the use of both elements is directly associated with the users of the building, it has been decided to take into account the state variables representing these elements within the preliminary list of variables (Table 2). Finally, according to the statistical analysis, it can be concluded that the highest peak power demand

and variance is associated with the summer season mainly due to the use the HVAC system for cooling purposes [40].

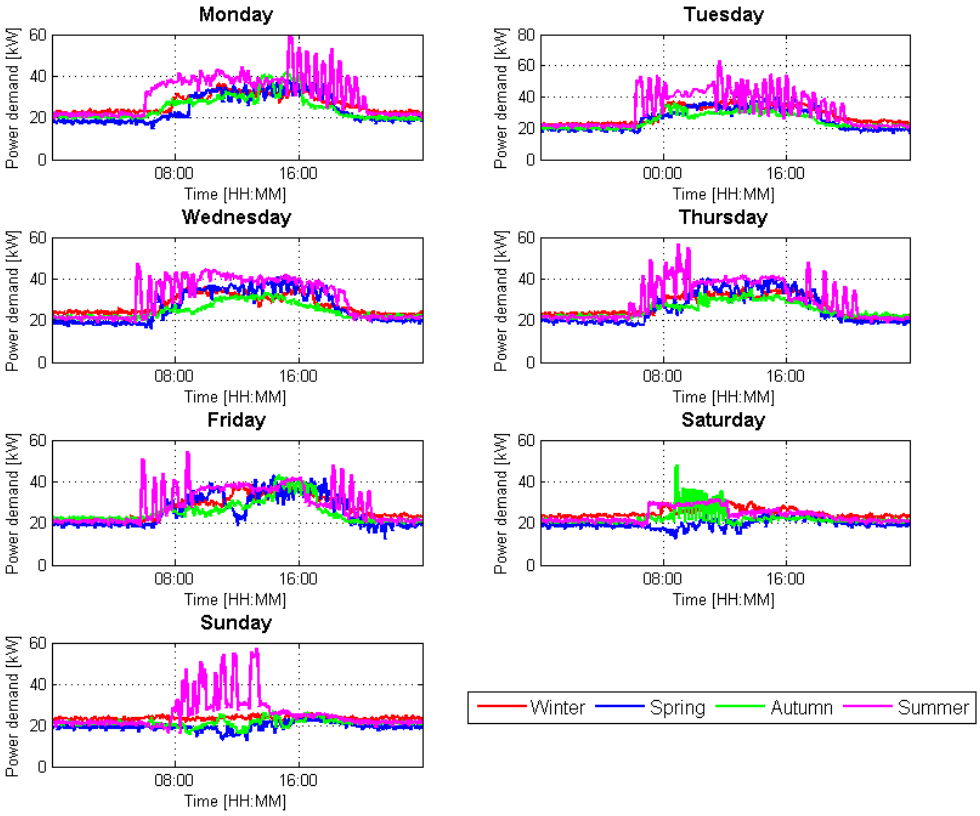

Figure 3. Weekly energy demand profiles for each season.

Table 2. Preliminary list of variables [17].

Variable	Unit	Measurement range
Type of the day (working day/non-working day)	-	(0, 1}
Hour of the day	-	[0,23]
Outdoor temperature	°C	[−5, 50]
Outdoor humidity	%	[0, ..., 100]
Outdoor solar radiation	W/m^2	[0,1440]
Outdoor wind speed	m/s	[0,22]
Outdoor wind direction	°	[0,360]
State of the pump B1.1 (off/on)	-	(0, 1)
State of the pump B1.2 (off/on)	-	(0, 1)
State of the pump B2.1 (off/on)	-	(0, 1)
State of the pump B2.2 (off/on)	-	(0, 1)
State of the pump B3.1 (off/on)	-	(0, 1)
State of the pump B3.2 (off/on)	-	(0, 1)
State of the pump B7 (off/on)	-	(0, 1)
State of the boiler (off/on)	-	(0, 1)
State of the absorption machine (off/on)	-	(0, 1)
State of the refrigeration tower (off/on)	-	(0, 1)
State of the heat pump (off/on)	-	(0, 1)
Electric power demand	kW	[0,85]
Electric power injected by the PV plant	kW	[0,9]

Finally, the principal conclusions which have been reached after this precise analysis can be summarized in: (a) there is a clear power demand profile within a week and also, differences between

working and non-working day power demand profiles can be undoubtedly established; (b) the power demand for summer is higher mainly due to the typical semi-desertic Mediterranean climate of Almería; and (c) the use of the solar cooling installation has a considerable influence on the final energy consumption.

2.2. Data-Sets Construction

As mentioned previously, in this paper, several energy consumption prediction models based on artificial neural networks (ANN) have been compared. These models have been obtained by means of different methodologies. More specifically, an ANN based prediction model using a MOGA [42,43] has been obtained. Afterwards, this model has been compared with a basic ANN model presented in [17]. To do that, a historic data set acquired at the CIESOL building has been used. Concretely, this data set comprises data from 1 September 2010 to 29 February 2012 with a sample time of 1 min and it includes a preliminary list of variables which can be observed in Table 2. These variables are related with the environmental conditions and the state of the main energy consuming elements of the solar cooling installation.

Subsequently, the selected data set has been split into three different balanced data subsets which have been used to train, test and validate the proposed ANN models. This division has been performed by hand since there were some discontinuities in time series. More information about the methodology followed to obtain these data subsets can be found in [17]. Thereafter, several procedures have been followed in order to obtain different prediction models. A description of these procedures is performed in the following sections.

3. A Non-Linear AutoRegressive with eXogenous Inputs Artificial Neural Network Model

In [17], a prediction model based on neural networks for the energy consumption of the CIESOL building was proposed. To do that, the neural network Toolbox™ provided by MATLAB® was used. Concretely, the proposed model had a non-linear autoregressive with eXogenous inputs (NARX) architecture, see Equation (1), typified by having a tapped delay line for the input signals set and another one for the output signal, that is, the power demand prediction of the CIESOL building. Moreover, this model has been trained using a gradient-descent based algorithm, more specifically the Levenberg-Marquardt algorithm [44]:

$$y\left[k+1\right] = \mathrm{f}\left(u\left[k\right], u\left[k-1\right], \ldots, u\left[k-d_u+1\right]; y\left[k\right], y\left[k-1\right], \ldots, y\left[k-d_y+1\right]\right) \quad (1)$$

In the previous equation, $u\left[k\right]$ and $y\left[k\right]$ represent the input and output signals at time instant k, $d_u \geqslant 1$, $d_y \geqslant 1$ (subject to $d_y \geqslant d_u$) are the memory orders for the input and output tapped delay lines, respectively, and f represents a non-linear mapping function which, in this case, has been approximated by a multilayer perceptron.

Finally, it can be established that the structure of the ANN is completely defined by indicating: (a) the number of hidden layers and the number of neurons in each of them; (b) the number of neurons in the output layer; and (c) the activation function used in each neuron of the hidden and output layers. More specifically, in the model presented in [17], an ANN with only one hidden layer composed by ten neurons with tangent hyperbolic activation functions and one neuron with linear activation function at the output layer has been used, since it is a universal approximator [45].

Afterwards, the selection of input variables from the preliminary variables list, see Table 2, was performed through analytical methods, since they allow to establish the existing linear and non-linear dependencies. Besides, scatter-plots and model tests have been used in order to complete the information provided by analytical methods. A detailed description of these methods can be found in [17]. Therefore, after the application of the methods which have just been mentioned, the preliminary variables list has been reduced to the following ones: type of the day; hour of the day; outdoor temperature and solar radiation; state variables related to the solar cooling installation; and the total power demand of the CIESOL building.

Finally, it is necessary to select the order of the signal inputs, that is, the embedding delay τ and the embedding dimension d [17]. The former has been determined by means of the average mutual information [46], whereas for the latter, optimal values were calculated by the false neighbors method [47]. The list of final input variables and their order can be observed in Table 3.

Table 3. Final list of variables with their order (embedding delay and dimension).

Variable	Unit	Measurement Range	τ	d
Type of the day (working day/non-working day)	-	(0, 1)	1	1
Hour of the day	-	[0,23]	1	1
Outdoor temperature	°C	[−5, 50]	1	4
Outdoor solar radiation	W/m^2	[0,1440]	1	4
State of the pump B1.1 (off/on)	-	(0, 1)	1	5
State of the pump B1.2 (off/on)	-	(0, 1)	1	5
State of the pump B2.1 (off/on)	-	(0, 1)	1	5
State of the pump B2.2 (off/on)	-	(0, 1)	1	5
State of the pump B3.1 (off/on)	-	(0, 1)	1	5
State of the pump B3.2 (off/on)	-	(0, 1)	1	5
State of the pump B7 (off/on)	-	(0, 1)	1	5
State of the boiler (off/on)	-	(0, 1)	1	5
State of the absorption machine (off/on)	-	(0, 1)	1	5
State of the refrigeration tower (off/on)	-	(0, 1)	1	5
State of the heat pump (off/on)	-	(0, 1)	1	5
Electric power demand	kW	[0,100]	1	3

4. Artificial Neural Network Based Models Generated by Multi Objective Genetic Algorithm

MOGA is a design framework implemented in MATLAB®, Python, and C programming languages, which can be applied to determine both the structure and the parameters of ANN based models. In this approach, instead of one model, a non-dominated set of models are generated. From this set, one solution must be selected. In this section the main concepts of MOGA and its application in ANN based models design are addressed. Afterwards, data preparation for MOGA and related experiments are described.

4.1. Multi Objective Genetic Algorithm

In the real world, the optimization of an engineering problem is a complicated task due to the presence of multiple objectives which, most of time, are conflicting with each other, meaning that improving one may deteriorate the other. In this case, there is a Pareto-optimal or non-dominated set in which each solution is not better than the other with respect to the multiple objectives. Figure 4 shows an example of a two objective minimization problem. The whole space of solutions is divided into two groups: the shaded region presents the dominated solutions while the solid curve illustrates the non-dominated set of solutions regarding objectives obj.1 and obj.2. As can be seen in Figure 4, A and B denote two non-dominated solutions.

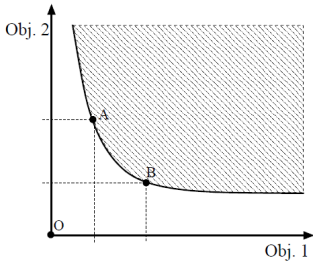

Figure 4. Bi-objective minimization problem. The shaded region presents dominated solutions and solid curve illustrates non-dominated solutions [51].

The goal of a multi-objective optimizer is to improve the surface of non-dominated solutions (*i.e.*, the solid curve) in such a way that the surface approaches the origin (*i.e.*, point 'O' in Figure 4) as much as possible.

Genetic algorithms (GA) are considered promising methods to deal with multi-objective optimization problems [48–50]. In MOGA, each individual in the population is evaluated in the space of the multiple objectives rather than in one objective. In addition, at the end of one run of the MOGA, a set of solutions is provided instead of one solution.

Since each individual is evaluated in multi-objective space, the value of objectives should be integrated into a single value in order to assign a fitness to the individual. A simple way is assigning weights to objectives so that each weight reflects the relative importance of its corresponding objective. Afterwards, the summation of the weighted objective's values is considered as a single value to compute and assign a fitness value to the individual. Selecting inappropriate weights leads to wrong searches; additionally, a small variation in weights may result in large changes in objectives.

As a proper alternative, an efficient Pareto-based ranking method has been proposed in [51]. In this way, each individual is ranked based on the number of individuals by which they are dominated. For non-dominated individuals, rank 0 is considered. In most applications, goals and priorities are defined for the objectives so that the Pareto-based ranking method should be modified. For more details about this method, please refer to [51].

4.2. Neural Network Based Model Design by Multi Objective Genetic Algorithm

The problem of designing a neural network based model can be divided into two sub-problems as follows:

Neural network structure: the network inputs and the number of hidden layers/neurons in the network;

Neural network parameters: they depend on the model chosen and are usually determined by a suitable training algorithm.

In this case a radial-basis function (RBF) Neural Network (NN) will be used. The output of a RBF model is given by:

$$o\left[k\right] = w_{l+1} + \sum_{j}^{l} w_j e^{-\frac{\| \, i[k] - \mathbf{C}(j) \, \|_2^2}{2\sigma_j^2}} \tag{2}$$

In Equation (2), $o\left[k\right]$ denotes the output, at instant k, $i_j\left[k\right]$ is the j^{th} input at that instant, w represents the vector of the linear weights, $\mathbf{C}\left(j\right)$ represents the vector (extracted from the $\mathbf{C}$ matrix) of the centers associated with the hidden neuron j, σ_j is its spread, and $\| \, \|_2$ represents the Euclidean distance. The network parameters, which will be denoted as the parameter vector $\mathbf{p}$, are therefore $\mathbf{C}$, σ and w.

According to the above sub-problems, in order to design a neural network based model that satisfies a set of defined goals, it is necessary to define a set of quality measures in the form of objectives for each sub-problem.

Assume that $D = (X, y)$ is a data set composed of N input-output pairs, which is divided into a training set, D^{t}, a generalization or testing set D^{g}, and a validation set D^{v}. Assume also that F is a set of all possible input features (delayed values of the modelled and exogenous variables) and $\mathbf{p}$ is the parameter vector. The problem of designing a neural network based model by MOGA can be expressed as follows:

Dataset D, the range $d \in [d_{\text{m}}, \ d_{\text{M}}]$ of input features from F and the range $n \in [n_{\text{m}}, \ n_{\text{M}}]$ of hidden neurons are given to the MOGA. After executing, the MOGA generates a non-dominated set of RBF models that minimize $\left[\mu_{\text{p}}, \mu_{\text{s}}\right]$ where μ_{p} and μ_{s} denote a set of objectives related to the neural network parameters $\mathbf{p}$ and the neural network structure, respectively.

In our work, the corresponding objectives for μ_p and μ_s were considered as follows:

$$\mu_p = \left[\varepsilon\left(D^t\right),\ \varepsilon\left(D^g\right), \varepsilon\left(D^s, PH\right)\right] \tag{3}$$

$$\mu_s = \left[O\left(\mu\right)\right] \tag{4}$$

where $\varepsilon\left(D^t\right)$ and $\varepsilon\left(D^g\right)$ denote the root-mean-square errors (RMSE) of the training set D^t and the testing set D^g, respectively. Consider a given prediction horizon (PH) and a simulation set D^s (with m consecutive input-output pairs). Assuming that $\mathbf{E}\left(D^s, PH\right)$ is an error matrix:

$$\mathbf{E}\left(D^s, PH\right) = \begin{bmatrix} e\left[1,1\right] & e\left[1,2\right] & \cdots & e\left[1,PH\right] \\ e\left[2,1\right] & e\left[2,2\right] & \cdots & e\left[2,PH\right] \\ \vdots & \vdots & \ddots & \vdots \\ e\left[m-PH,1\right] & e\left[m-PH,1\right] & \cdots & e\left[m-PH,PH\right] \end{bmatrix} \tag{5}$$

where $e\left[i,j\right]$ is the model prediction error taken from instant i of D^s at step j within the PH. By denoting $\rho\left(.,i\right)$ as the RMS function operating over the i^{th} column of its argument matrix, then $\varepsilon\left(D^s, PH\right)$ is defined as:

$$\varepsilon\left(D^s, PH\right) = \sum_{i=1}^{PH} \rho\left(\mathbf{E}\left(D^s, PH\right), i\right) \tag{6}$$

$O\left(\mu\right)$ denotes the model complexity, which is equal to the number of input features + 1, multiplied by the number of hidden neurons, reflecting the RBF input-output topology.

The MOGA searches the space spanned by the number of neurons and the input features, *i.e.*, the model structure. Each individual in the population has a chromosome representation consisting of two components. The first corresponds to the number of hidden neurons The second component is a string of integers, each one representing the index of a particular feature in F. The chromosome representation is shown in Figure 5.

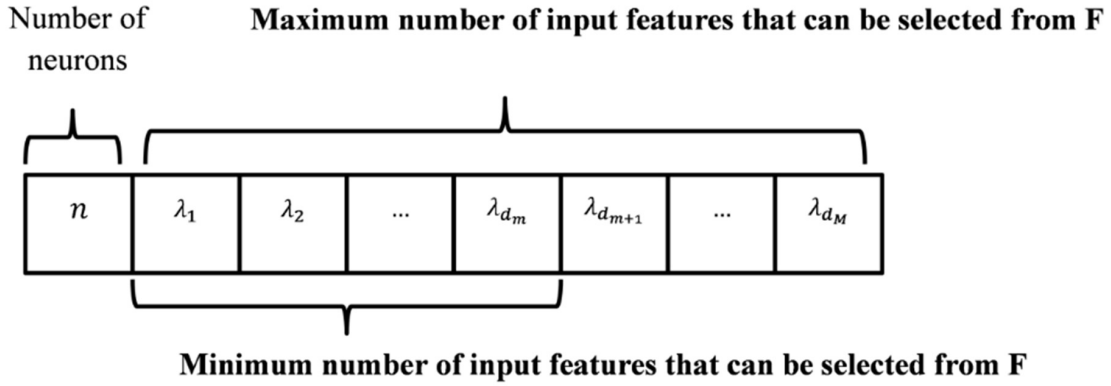

Figure 5. Chromosome representation.

Before being evaluated in the MOGA, each model has its parameters determined by a Levenberg-Marquardt algorithm [37] minimizing an error criterion that exploits the linear-nonlinear relationship of the RBF NN model parameters [52–54]. The initial values of the nonlinear parameters ($\mathbf{C}$ and σ) are chosen randomly, or with the use of a clustering algorithm, $\mathbf{w}$ is determined as a linear least-squares solution, and the procedure is terminated using the early-stopping approach [55] within a maximum number of iterations.

4.3. Model Design Cycle

Briefly, the model design optimization problem is a sequence of actions which are undertaken by the model designer. These actions are repeated until the pre-specified design goals are achieved. There are three main actions in model design cycle: problem definition, solution(s) generation and analysis of results. In the problem definition stage, the datasets, the ranges of features and neurons are defined, as well as the objectives. After this stage, the MOGA does a guided search to obtain models that satisfy the predefined objectives and goals. In the third stage, the set of models obtained that lie in the Pareto front are analyzed. In this set, the performance of the models in the validation set (not involved in the design) is of paramount importance. If good solutions are found, the process stops. Otherwise, based on the results analysis, the search space can be reduced, and/or the objectives and goals can be redefined, therefore restricting the trade-off surface coverage. A more detailed description of the MOGA based ANN design framework can be found, for instance, in [43].

4.4. Data Preparation

After an analysis of the original data, a new code was considered for the feature "day type". The new code refers to "special days". By comparing the amount of energy consumption for working and non-working days, it has been revealed that for some days over the years 2010 and 2011, the amount of energy consumption has an average value between working and non-working days. By comparing these special days with the Spanish calendar for both years, it was found that those days occurred in the early days of the year, or in working days which were located between national/regional holidays and weekends. Based on that, these special days received the code 0.5. Figure 6 shows the distribution of whole data samples in terms of "day type".

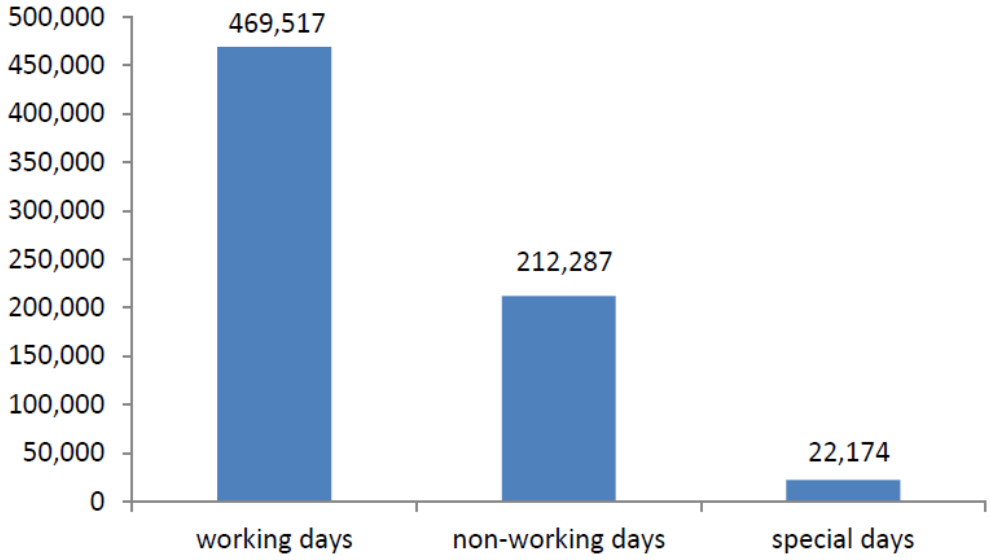

Figure 6. Distribution of original data samples in terms of day type from 1 September 2010 to 29 February 2012.

Since the original data was obtained with a sampling interval of 1 min, its size was too large (514,762 samples) to be handled by the MOGA framework, and was reduced in several stages. Due to presence of gaps in the data, there were 51 consecutive periods over the whole data. In the first stage, each period was divided into one week length segments. Based on these divisions, those durations whose length was less than two weeks were ignored in this work. This stage resulted into 13 periods containing at least two weeks of data. Table 4 shows the periods selected in the first stage.

In the second stage, the data for all periods was reduced by a factor of 15 by averaging every 15 consecutive samples inside each segment. The sampling interval was then increased to 15 min.

Table 4. The periods selected in the first stage.

Period Number	Start	End
1	2 September 2010 00:00:00	15 September 2010 23:59:00
2	24 September 2010 00:00:00	14 October 2010 23:59:00
3	9 November 2010 00:00:00	22 November 2010 23:59:00
4	27 December 2010 00:00:00	9 January 2011 23:59:00
5	11 January 2011 00:00:00	31 January 2011 23:59:00
6	9 February 2011 00:00:00	1 March 2011 23:59:00
7	11 March 2011 00:00:00	31 March 2011 23:59:00
8	2 June 2011 00:00:00	22 June 2011 23:59:00
9	8 July 2011 00:00:00	1 September 2011 23:59:00
10	14 October 2011 00:00:00	27 October 2011 23:59:00
11	5 November 2011 00:00:00	23 December 2011 23:59:00
12	29 December 2011 00:00:00	11 January 2012 23:59:00
13	19 January 2012 00:00:00	8 February 2012 23:59:00

In the third stage, by starting from the second week within each period, three random days along with the last seven consecutive days were selected as lags for each variable. This way, a data set D with 8640 samples was obtained. Figure 7 shows the distribution of samples of data set D in terms of "day type".

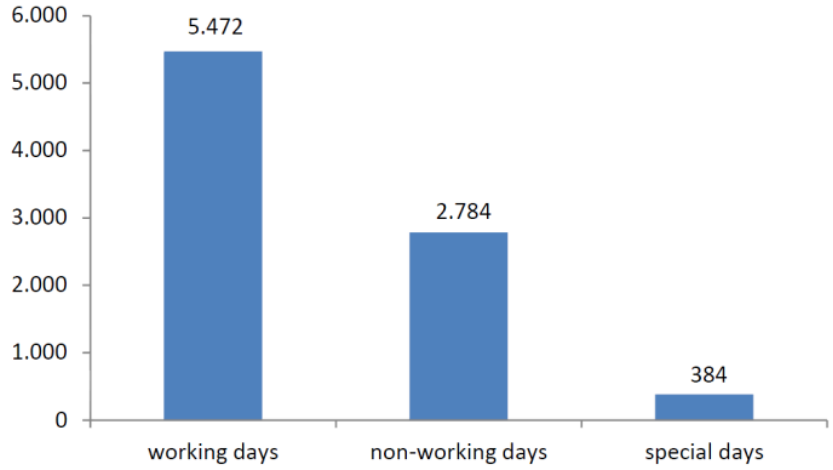

Figure 7. Distribution of samples in data set D in terms of day type.

4.5. Design Experiments

Based on the model design cycle described in Section 4.3, several designs were conducted in such a way that their results led to the definition of a new design, by redefining variables and their corresponding lag terms, as well as imposing restrictions on objectives.

In a first step, we conducted designs with features requiring lag terms spread over at most 7 days. After analyzing and comparing the results with those obtained in [17], the spread of lags was reduced to cover at most 2 days, and finally to cover at most one day. Based on that, four new designs were carried out.

For all designs, data set D, stated in Section 4.4, containing 8640 samples was used. Since a sampling interval of 15 min was used, and the objective was to obtain forecasts of electric power 1 h-ahead, a prediction horizon of four steps was employed. In this work, as in [17], two groups of models were considered. The first group contains simple models where only weather variables are used as exogenous variables. The second group considers complete models involving both weather and solar cooling operation variables. The list of candidate variables used and the range of lags for the design experiments are given in Tables 5 and 6 respectively.

Table 5. List of variables used.

Variable	Notation	Unit	Range in D
Electric power demand added up with the electric power supplied by the PV plant	$x1$	kW	[11.73, 74.65]
Day type (working day/non-working day/semi-holidays)	$x2$	-	(0, 0.5, 1)
Outdoor temperature	$x3$	°C	[2.73, 43.79]
Outdoor solar radiation	$x4$	W/m^2	[0, 1127.81]
State of pump B1.1 (off/on)	$x5$	-	(0, 1)
State of Pump B1.2 (off/on)	$x6$	-	(0, 1)
State of Pump B2.1 (off/on)	$x7$	-	(0, 1)
State of Pump B2.2 (off/on)	$x8$	-	(0, 1)
State of Pump B7 (off/on)	$x9$	-	(0, 1)
State of the boiler (off/on)	$x10$	-	(0, 1)
State of the absorption machine (off/on)	$x11$	-	(0, 1)
State of the cooling tower (off/on)	$x12$	-	(0, 1)
State of the heat pump (off/on)	$x13$	-	(0, 1)

Table 6. Description of the lags used.

Variable	Experiment I	Experiment II	Experiment III	Experiment IV
$x1$	20 lags over 1 day	20 lags over 1 day	20 lags over 1 day	20 lags over 1 day
$x2$	0 lags	0 lags	0 lags	0 lags
$x3$	20 lags over 1 day	20 lags over 1 day	20 lags over 1 day	20 lags over 1 day
$x4$	20 lags over 1 day	20 lags over 1 day	20 lags over 1 day	20 lags over 1 day
$x5$	-	-	1 lag	1 lag
$x6$	-	-	1 lag	1 lag
$x7$	-	-	1 lag	1 lag
$x8$	-	-	1 lag	1 lag
$x9$	-	-	1 lag	1 lag
$x10$	-	-	1 lag	1 lag
$x11$	-	-	1 lag	1 lag
$x12$	-	-	1 lag	1 lag
$x13$	-	-	1 lag	1 lag

As it can be seen in Table 6, Experiments I and II correspond to simple models in which only weather variables have been used; Experiments III and IV consider complete models. In Table 6, "lag 0" for variable "day type" ($x2$) is translated into the day type of instant $k+1$ for which the electric power demand is predicted. In fact, weather and electric power demand variables are strongly related to their most recent values and also, to a certain extent, to their values 24 h before. As a result, for $x1$, $x3$ and $x4$ a heuristic, proposed in [43], was used to select 20 lags over one full day, in such a way that more recent values predominate in the set of searchable lags for these variables. Hence, based on this heuristic, the 20 lags used are [1–7, 9, 11, 13, 16, 20, 24, 29, 36, 43, 53, 65, 79, 96] . In this list, and as an example, lags 1 and 2 denote delays of 15 and 30 min, respectively. The objectives and the corresponding goals are given in Table 7.

Table 7. Objectives and their corresponding restriction of experiments.

Objectives	Experiment I	Experiment II	Experiment III	Experiment IV
$\varepsilon\left(D^{t}\right)$	Minimize	<0.059	Minimize	<0.054
$\varepsilon\left(D^{g}\right)$	Minimize	<0.061	Minimize	<0.052
$\varepsilon\left(D^{s}, 16\right)$	Minimize	Minimize	Minimize	Minimize
$O\left(\mu\right)$	Minimize	<317	Minimize	<444

Regarding MOGA's design framework parameters specification, for experiments I and III, the range $[d_{\mathrm{m}},\ d_{\mathrm{M}}]$, where d_{m} and d_{M} are the minimum and maximum number of features, was set to [1, 30] while for experiments II and IV they were set to [1, 15] and [1, 21], respectively. Similarly, for experiments I and III, the range $[n_{\mathrm{m}},\ n_{\mathrm{M}}]$, where n_m and n_{M} are the minimum and maximum number of neurons, was set to [2,30] while for experiments II and IV, these ranges were set to [1, 18] and [1, 21], repectively. For all designs, the population size and the number of generations were set to 100. For each experiment, a proper sub dataset D^{W} was derived from data set D whose features are those columns of D which correspond to the lags defined in the corresponding experiment.

In order to generate training, testing and validation sets for each experiment, firstly the ApproxHull algorithm [56] was applied on corresponding D^{W} to obtain convex points reflecting the whole input range in which the model is supposed to be used. Secondly, 50% of whole samples in D^{W} were used to generate training, testing and validation sets with proportions of 60%, 20% and 20%, respectively. In this step all convex points were incorporated in the training set. Afterwards, the remaining samples were shared randomly into the rest of the training set, and the testing and validation sets. Regarding the simulation dataset D^{s}, 1344 consecutive samples from 1 October 2010 00:00:00 to 14 October 2010 23:59:00 were considered. In this set, the rows correspond to the variables used, whose samples are in each column while, for the other sets, the number of rows correspond to the patterns, and the number of columns to the features. The size of training, testing and validation datasets as well as the simulation dataset of each experiment is given in Table 8.

After one run of the MOGA for each experiment, the non-dominated and preferred sets of models were generated. In the case that no restriction is considered on objectives, the non-dominated set is the same as preferred set; otherwise, the preferred set is a subset of the non-dominated set whose solutions satisfy the goals. Please refer to [51] for further information about how the preferred set can be obtained from the non-dominated set by applying the preferably criterion. The number of models in non-dominated and preferred sets for each experiment is given in Table 9.

Table 8. Size of training, testing and validation sets.

Data set	Experiment I	Experiment II	Experiment III	Experiment IV
D^{t}	2592 × 62	2592 × 62	2592 × 71	2592 × 71
D^{g}	864 × 62	864 × 62	864 × 71	864 × 71
D^{v}	864 × 62	864 × 62	864 × 71	864 × 71
D^{s}	4 × 1344	4 × 1344	13 × 1344	13 × 1344

Table 9. Size of non-dominated and preferred sets.

Experiment	Non-dominated set	Preferred set
Experiment I	346	346
Experiment II	238	88
Experiment III	289	289
Experiment IV	366	182

5. Results and Discussion

The models presented in this paper have been tested and compared by means of real data acquired at the CIESOL building. To do that, a battery of tests has been selected according to certain representative characteristics, such as, the type of day (working and non-working days), the season of the year and the quantity of solar radiation (sunny and cloudy days). A complete description of the battery of tests is shown in Table 10. Furthermore, a prediction horizon over 1 h has been set mainly due to the energy price changes and the dynamic behaviour of indoor temperature [17].

Since in MOGA related experiments, the data used a sampling interval of 15 min, each test in Table 10 contains 96 samples. Moreover, the corresponding prediction horizon over 1 h is equal to

four steps. For the model proposed in [17], each test includes 1440 samples due to the 1 min sampling rate. Hence, the corresponding prediction horizon over 1 h is equal to 60 steps. For convenience, the complete model proposed in [17] and the models obtained by MOGA will be denoted as PREVIOUS and MOGA models, respectively. In order to compare the MOGA models obtained from each experiment with the PREVIOUS model, one model was selected from the non-dominated/preferred set, with a good compromise between performance and complexity.

Table 10. Battery of tests performed.

Test	Day	Temperature	Radiation	Date
(A)	Working day	Summer	Sunny	29 June 2011
(B)	Non-working day	Summer	Sunny	19 September 2010
(C)	Working day	Winter	Cloudy	15 February2011
(D)	Non-working day	Winter	Sunny	20 February 2011
(E)	Non-working day	Winter	Cloudy	28 February 2011
(F)	Non-working day	Summer	Cloudy	2 July 2011

In our work, models I–IV were the selected MOGA models from experiments I–IV, respectively. Information about the selected MOGA models as well as the PREVIOUS is given in Table 11. Using the notation of Table 6, the formal description of models I–IV is given by Equations (7)–(10), respectively:

$$\hat{y}(k+1) = \mathrm{f}_1(x_1(k), \ldots, x_1(k-6), x_1(k-8), x_1(k-11), x_1(k-12), x_1(k-19), x_2(k+1), x_3(k-2), x_3(k-7), x_3(k-10), x_4(k-4), x_4(k-10), x_4(k-17)) \quad (7)$$

$$\hat{y}(k+1) = \mathrm{f}_2(x_1(k), \ldots, x_1(k-4), x_1(k-6), x_1(k-9), x_1(k-10), x_1(k-15), x_1(k-18), x_3(k-9), x_4(k), x_4(k-8), x_4(k-18)) \quad (8)$$

$$\hat{y}(k+1) = \mathrm{f}_3(x_1(k-1), x_1(k-3), x_1(k-4), x_1(k-5), x_1(k-7), x_1(k-10), x_1(k-11), x_1(k-12), x_1(k-14), x_1(k-15), x_1(k-16), x_2(k+1), x_3(k), x_3(k-2), x_3(k-3), x_3(k-4), x_3(k-8), x_3(k-12), x_3(k-13), x_3(k-15), x_3(k-16), x_4(k-2), x_4(k-3), x_4(k-5), x_4(k-7), x_4(k-12), x_7(k), x_{11}(k), x_{13}(k)) \quad (9)$$

$$\hat{y}(k+1) = \mathrm{f}_4(x_1(k), x_1(k-1), x_1(k-2), x_1(k-3), x_1(k-5), x_1(k-17), x_2(k+1), x_3(k-18), x_4(k-3), x_4(k-5), x_4(k-10), x_4(k-14), x_4(k-15), x_4(k-18), x_9(k), x_{10}(k), x_{11}(k), x_{13}(k)) \quad (10)$$

$\hat{y}(k+1)$ in Equations (7)–(10) is the output of the corresponding RBF neural network, representing $o[k]$ in Equation (2). Each function f_j , $\{j = 1, 2, 3, 4\}$ has its own set of input terms. These input terms, all together, constitute the input data sample at instant k corresponding to $\boldsymbol{i}[k]$ in Equation (2).

Table 11. Selected multi objective genetic algorithm (MOGA) models and PREVIOUS model. Artificial neural networks: ANN.

Model	Number of features	Number of neurons	Complexity
Model I	18	13	247
Model II	14	18	270
Model III	29	11	330
Model IV	18	20	380
NARX-ANN	67	10	680

To compare MOGA models with the PREVIOUS model over the battery of tests stated in Table 10, five statistical criteria were considered: mean absolute error (*MAE*), mean relative error (*MRE*), Mean

absolute percentage error (*MAPE*), maximum absolute error (*MaxAE*) and standard deviation of predicted values (σ). These criteria can be calculated according to Equations (11)–(15):

$$MAE = \frac{1}{N}\sum_{i=1}^{N}|x(i) - \hat{x}(i)| \tag{11}$$

$$MRE = \frac{1}{N}\sum_{i=1}^{N}\frac{|x(i) - \hat{x}(i)|}{x(i)} \tag{12}$$

$$MAPE = \frac{100\%}{N}\sum_{i=1}^{N}\frac{|x(i) - \hat{x}(i)|}{|x(i)|} \tag{13}$$

$$\mathrm{Max}AE = \max\left(AE\left(x, \hat{x}\right)\right) \tag{14}$$

$$\sigma = \sqrt{\frac{1}{N}\sum_{i=1}^{N}\left(\hat{x}(i) - \overline{\hat{x}}(i)\right)^2} \tag{15}$$

In Equations (11)–(15), N, x and $\hat{x}$ denote the number of samples, measured values and predicted values of the variable, respectively. The evaluations of MOGA and PREVIOUS models over the battery of tests for a prediction horizon of 1 h are given in Tables 12–17. The best values for each criterion are identified in bold.

Regarding test A, a working sunny day in summer, Model I, as a simple model, not only has minimum values in terms of *MAE*, *MRE* and *MAPE* among other MOGA models but also has a better performance than PREVIOUS in terms of these criteria. In this test, in overall, simple models I and II have better performance in comparison with complete models III and IV.

Table 12. Results obtained by MOGA and PREVIOUS models over Test A, for a prediction horizon (*PH*) of 1 h. Mean absolute error (*MAE*); mean relative error (*MRE*); mean absolute percentage error (*MAPE*); maximum absolute error (Max*AE*).

Parameter	Model I	Model II	Model III	Model IV	PREVIOUS
MAE (kW)	**1.92**	2.14	2.28	3.55	1.96
MRE (kW)	**0.06**	0.08	0.07	0.12	**0.06**
MAPE (%)	**6.29**	8.11	7.66	12.39	6.38
Max*AE* (kW)	12.36	14.22	**10.21**	13.82	10.99
σ (kW)	8.92	7.86	8.91	**6.99**	7.17

Table 13. Results obtained by MOGA and PREVIOUS models over Test B, for a *PH* of 1 h.

Parameter	Model I	Model II	Model III	Model IV	PREVIOUS
MAE (kW)	0.95	1.22	1.29	0.93	**0.84**
MRE (kW)	0.05	0.07	0.07	**0.05**	**0.05**
MAPE (%)	5.60	7.21	7.86	5.80	**5.13**
Max*AE* (kW)	3.60	**3.15**	4.83	3.38	3.59
σ (kW)	2.01	2.48	1.78	1.75	**1.52**

Table 14. Results obtained by MOGA and PREVIOUS models over Test C, for a *PH* of 1 h.

Parameter	Model I	Model II	Model III	Model IV	PREVIOUS
MAE (kW)	1.99	3.46	**1.75**	1.95	1.86
MRE (kW)	0.06	0.1	**0.06**	**0.06**	**0.06**
MAPE (%)	6.62	10.55	**6.25**	6.40	6.26
Max*AE* (kW)	8.82	16.56	**5.69**	7.04	8.15
σ (kW)	**6.04**	6.94	6.78	7.75	6.70

Table 15. Results obtained by MOGA and PREVIOUS models over Test D, for a *PH* of 1 h.

Parameter	Model I	Model II	Model III	Model IV	PREVIOUS
MAE (kW)	0.94	1.12	**0.82**	0.88	1.08
MRE (kW)	0.04	0.05	**0.03**	0.04	0.05
MAPE (%)	4.21	5.34	**3.81**	4.17	4.86
Max*AE* (kW)	**4.65**	6.35	5.20	5.45	6.28
σ (kW)	1.95	1.64	**1.08**	1.72	1.52

Table 16. Results obtained by MOGA and PREVIOUS models over Test E, for a *PH* of 1 h.

Parameter	Model I	Model II	Model III	Model IV	PREVIOUS
MAE (kW)	1.38	1.45	**1.16**	1.30	1.49
MRE (kW)	0.06	0.06	**0.05**	**0.05**	0.06
MAPE (%)	6.00	6.30	**5.06**	5.77	6.38
Max*AE* (kW)	**4.44**	5.59	4.81	4.49	6.89
σ (kW)	1.80	1.39	**1.28**	1.65	1.43

Table 17. Results obtained by MOGA and PREVIOUS models over Test F, for a *PH* of 1 h.

Parameter	Model I	Model II	Model III	Model IV	PREVIOUS
MAE (kW)	1.02	**0.80**	1.35	0.89	0.95
MRE (kW)	0.04	**0.03**	0.06	0.04	0.04
MAPE (%)	4.87	**3.70**	6.53	4.28	4.31
Max*AE* (kW)	3.43	**2.63**	5.68	3.73	3.75
σ (kW)	1.95	1.99	**1.44**	1.97	1.88

With respect to test B, a non-working sunny day in summer, Model IV, as a complete model, has minimum values of *MAE*, *MRE* and σ in comparison with other MOGA models; with respect to *MaxAE*, it has a compromise performance between Model II and PREVIOUS.

In test C, a working cloudy day in winter, and in test D, a non-working sunny day in winter, the complete model III has minimum values in terms of *MAE*, *MAPE* and Max*AE* among all models. Model I, a simple model, has also a good performance; actually better in 4 criteria than the complete PREVIOUS model, in test D.

In test E, a non-working cloudy day in winter, both simple and complete MOGA models have lower values in terms of *MAE*, *MAPE* and Max*AE* than the PREVIOUS model. Model III has better performance in all criteria.

Regarding test F, a non-working cloudy day in summer, simple model II and complete model IV have better performance in terms of *MAE*, *MAPE* and *MaxAE* than PREVIOUS model. In this comparison, model II has minimum values in all criteria, except σ.

According to Tables 12–17 in the group of simple models, model I, in most cases, has better performance than model II. In the group of complete models, model III, in most cases, is better than model IV. Figures 8–10 show the comparison between measured and predicted value of electric power demand in CIESOL building, over tests A–F for a prediction horizon of 1 h, for the PREVIOUS model, model I and III, respectively.

Comparing the performance of all MOGA models over the battery of tests, in general complete models III and IV have a better performance in winter than in summer, while simple model I has a compromise performance between summer and winter.

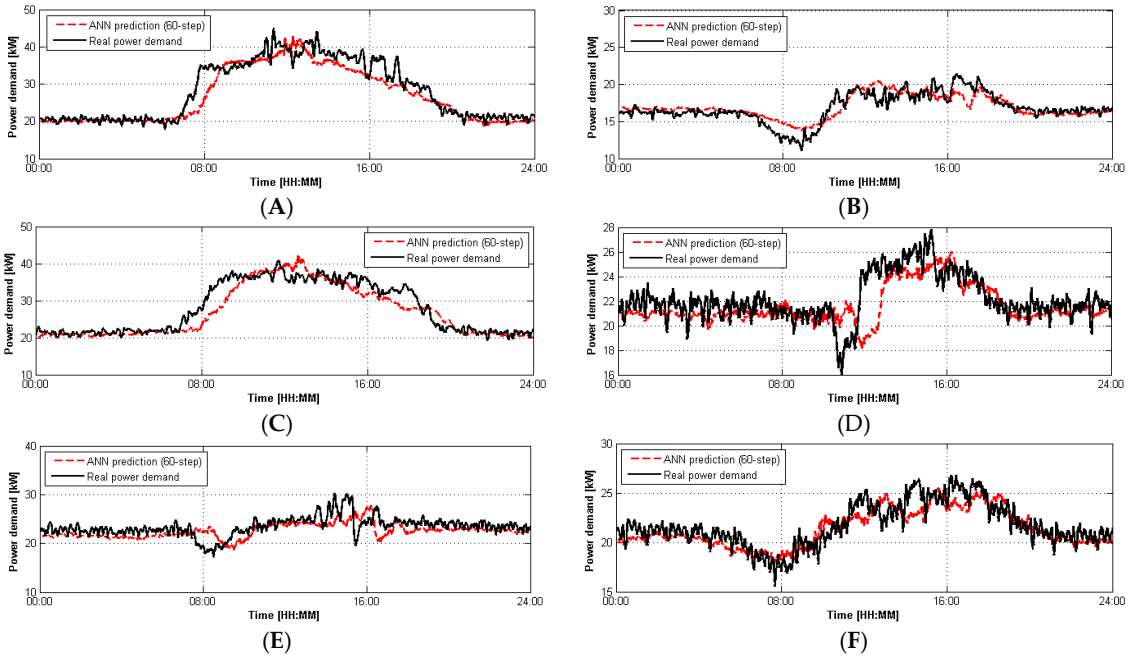

Figure 8. Prediction results for tests (**A**–**F**) using the PREVIOUS model.

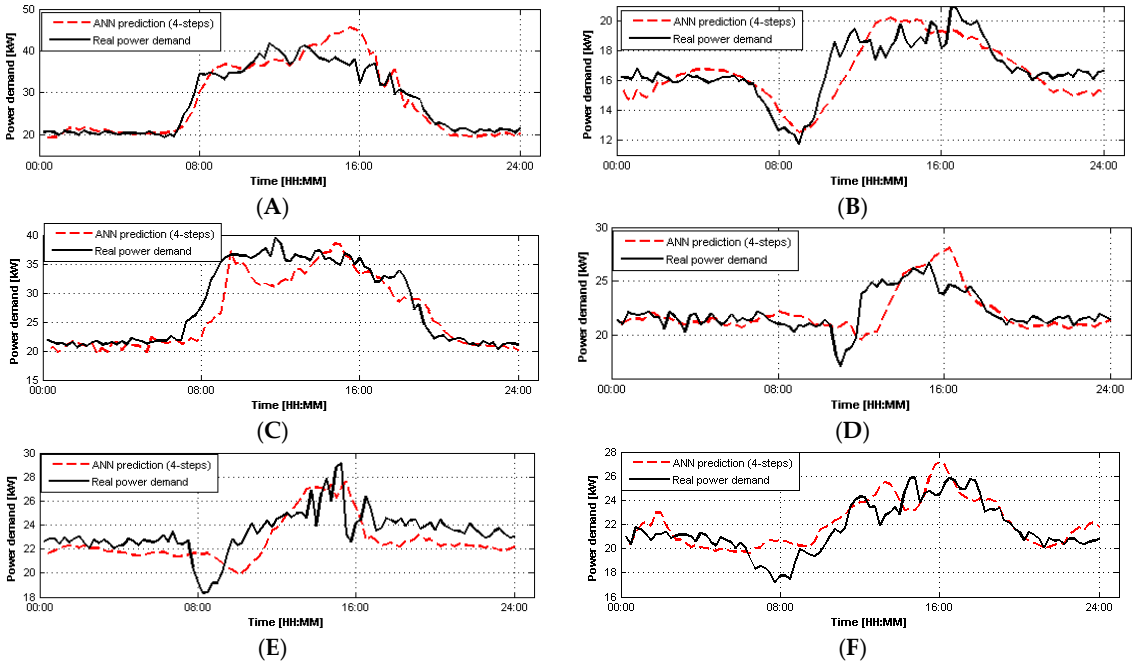

Figure 9. Prediction results for tests (**A**–**F**) using model I.

5.1. Comparison of Multi Objective Genetic Algorithm Models with Naive Autoregressive Baseline Approach

The performance of MOGA models was also compared with a NAB model, introduced in [38]. The NAB approach considers, as estimate of the electric power demand at instant k, the measured value of consumption at the corresponding instant of time, in the same day of the previous week. It is therefore a simple model which does not need any computation to predict electric power demand at each time instant k. To apply the NAB approach to tests A–F, consecutive data corresponding to the previous week would be needed. Since there were several gaps in the whole dataset among tests A–F, only for tests D and E, corresponding to special days in winter, consecutive data exist to implement

this method. In order to evaluate the NAB model in summer, we considered another special day in summer, corresponding to 6 August 2011, hereinafter called test G. For convenience, the description of the tests D, E and G is given in Table 18.

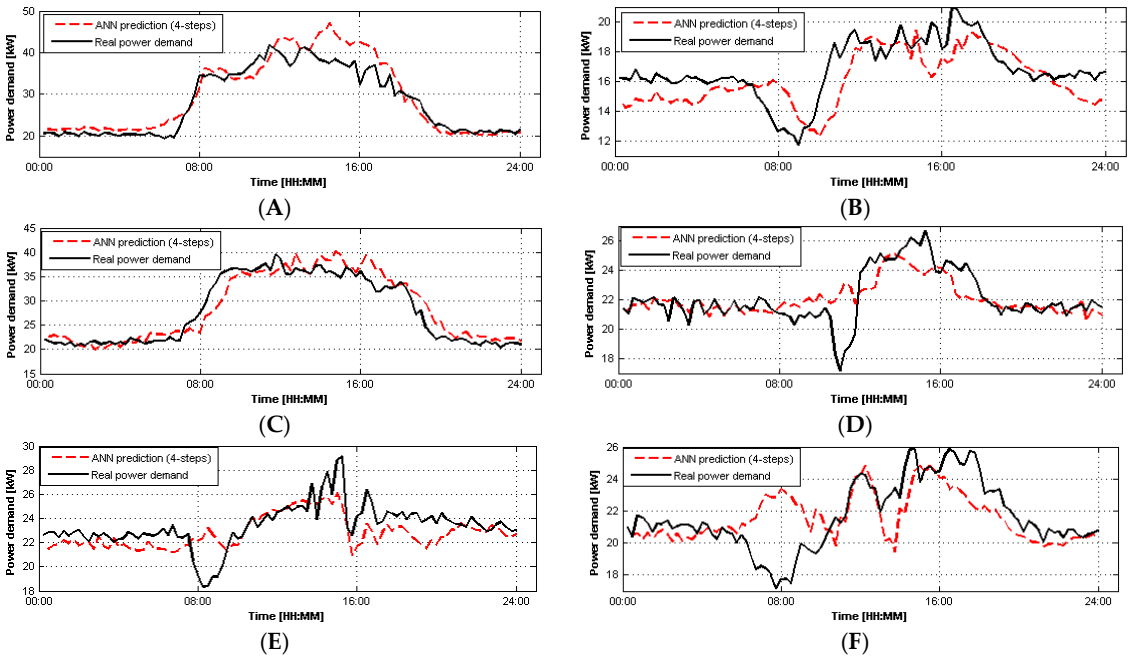

Figure 10. Prediction results for tests (**A**–**F**) using model III.

Table 18. Battery of tests performed to compare the naive autoregressive baseline (NAB) model with the neural networks models.

Test	Day	Temperature	Radiation	Date
(D)	Non-working day	Winter	Sunny	20 February 2011
(E)	Non-working day	Winter	Cloudy	28 February 2011
(G)	Non-working day	Summer	Sunny	6 August 2011

In order to compare the performance of NAB model with MOGA models and PREVIOUS model, the three models were evaluated over the battery of tests stated in Table 18. The results obtained over tests D, E and G are given in Tables 19–21. Please note that the results of MOGA models and PREVIOUS model, for tests D and E, are obtained from Tables 14 and 15 respectively, and are reproduced here for easy of comparison with the NAB approach.

Table 19. Results obtained by neural network and NAB models over Test D, for a *PH* of 1 h.

Parameters	Model I	Model II	Model III	Model IV	PREVIOUS	NAB
MAE (kW)	0.94	1.12	**0.82**	0.88	1.08	1.9439
MRE (kW)	0.04	0.05	**0.03**	0.04	0.05	0.0856
MAPE (%)	4.21	5.34	**3.81**	4.17	4.86	8.5575
Max*AE* (kW)	**4.65**	6.35	5.20	5.45	6.28	6.8341
σ (kW)	1.95	1.64	**1.08**	1.72	1.52	1.8933

Table 20. Results obtained by neural network and NAB models over Test E, for a *PH* of 1 h.

Parameters	Model I	Model II	Model III	Model IV	PREVIOUS	NAB
MAE (kW)	1.38	1.45	**1.16**	1.30	1.49	4.8314
MRE (kW)	0.06	0.06	**0.05**	**0.05**	0.06	0.2086
MAPE (%)	6.00	6.30	**5.06**	5.77	6.38	20.8610
MaxAE (kW)	**4.44**	5.59	4.81	4.49	6.89	13.0946
σ (kW)	1.80	1.39	**1.28**	1.65	1.43	5.6539

Table 21. Results obtained by neural network and NAB models over Test G, for a *PH* of 1 h.

Parameters	Model I	Model II	Model III	Model IV	PREVIOUS	NAB
MAE (kW)	0.8297	1.2684	0.8089	**0.7598**	0.7787	3.2966
MRE (kW)	0.0472	0.0745	0.0465	0.0434	**0.0432**	0.1909
MAPE (%)	4.7154	7.4521	4.648	4.3363	**4.3154**	19.0867
Max*AE* (kW)	3.7347	7.4701	4.7188	3.8647	**2.9473**	13.6549
σ (kW)	2.08	2.216	1.5135	**1.2575**	1.822	3.8805

Regarding these tests, the NAB model has the worst performance (by a large difference) in comparison to MOGA and PREVIOUS models, in terms of all criteria.

Regarding test G, a new test corresponding to a non-working sunny day in summer, Model IV, a complete model, has minimum values in terms of *MAE* and σ. In terms of *MRE* and *MAPE*, Model IV has approximately the same performance as PREVIOUS model. In the same way as in tests D and E, the NAB model has the worst performance.

6. Conclusions

Artificial intelligence techniques are promising tools for predicting the power consumption in buildings. In this study, we applied a MOGA framework to design RBF models for this purpose and compared the performance obtained by the designed models with an already existing multilayer perceptron predictive model, proposed in [17].

Both the MOGA and PREVIOUS models aimed to predict the electric power demand in the bioclimatic CIESOL building over a prediction horizon of 1 h. MOGA models employed a sampling interval of 15 min, therefore requiring a prediction horizon of four steps, while the PREVIOUS model employed a prediction horizon of 60 steps, as data was sampled with a 1 min rate.

Four MOGA models were designed and their performance was compared with the PREVIOUS model. Model I and II used only weather variables as exogenous variables while models III, IV and PREVIOUS employed, in addition to weather information, solar cooling operation variables. According to results obtained in a battery of tests, one can say that complete models III and IV have a better performance in winter than in summer, while the performance of model I as a simple model has a compromise performance in summer and winter.

Comparing the performance of MOGA models and the PREVIOUS, despite the fact that MOGA models were trained with a small training set of 2592 samples compared to the 318340 samples used to train the PREVIOUS model, they have obtained better results, except in Test B. Moreover, as it can be seen in Table 11, the complexity of models obtained from MOGA is lower than the PREVIOUS model. According to tests D, E and G reflecting special days in winter and summer, both MOGA and PREVIOUS models have much better performance than the NAB model in terms of all criteria.

Acknowledgments: Authors wish to thank the financial support provided by the Transnational Access to Research Infrastructures within the European project SFERA II (Grant Agreement N. 312.643) under the 7th Framework Program; the Project ENERPRO DPI2014-56364-C2-1-R financed by the Spanish Ministry of Economy and Competitiveness and EU-ERDF funds; the project OPTICONES financed by the IBERDROLA Spain Foundation within the framework of the 2015/16 call for Energy and Environment research grants and Portuguese Foundation for Science & Technology, through IDMEC, under LAETA, Project UID/EMS/50022/2013.

Author Contributions: All authors have participated in preparing the research from the beginning to the end, such as establishing research design, method and analysis. All authors discussed and finalized the analysis results to prepare manuscript according to the progress of research.

Conflicts of Interest: The authors declare no conflict of interest.

Nomenclature

Acronyms

ANN	Artificial neural network
ARIMA	Auto regressive integrated moving average
ARMA	Auto regressive moving average
CDA	Conditional demand analysis
CIEMAT	Centre for energy, environment and technology—Centro de Investigaciones Energéticas, MedioAmbientales y Tecnológicas (in Spanish)
CIESOL	Solar Energy Research Center—*Centro de Investigación en Energía SOLar* (in Spanish)
HVAC	Heating, ventilating and air conditioning
GMM	Gaussian mixture models
MOGA	Multi objective genetic algorithm
NAB	Naive autoregressive baseline
NARX	Non-linear autoregressive with eXogenous inputs
RBF	Radial-basis function
RMSE	Root mean square

Symbols

D^{t}	Training set
D^{g}	Testing set
D^{v}	Validation set
D^{s}	Simulation set
$\varepsilon\left(D^{t}\right)$	RMSE of D^{t}
$\varepsilon\left(D^{g}\right)$	RMSE of D^{g}
$E\left(D^{s}, PH\right)$	Error matrix over D^{s} within a prediction horizon PH
$\varepsilon\left(D^{s}, PH\right)$	Sum of root mean square of each column of $E\left(D^{s}, PH\right)$
MAE	Mean absolute error
MRE	Mean relative error
$MAPE$	Mean absolute percentage error
MaxAE	Maximum absolute error
$O\left(\mu\right)$	Model complexity

References

1. Perez-Lombard, L.; Ortiz, J.; Pout, C. A review on buildings energy consumption information. *Energy Build.* **2008**, *40*, 394–398. [CrossRef]
2. Nejat, P.; Jomehzadeh, F.; Taheri, M.M.; Gohari, M.; Majid, M.Z.A. A global review of energy consumption, CO_2 emissions and policy in the residential sector (with an overview of the top ten CO_2 emitting countries). *Renew. Sustain. Energy Rev.* **2015**, *43*, 843–862. [CrossRef]
3. Zhao, H.-X.; Magoules, F. A review on the prediction of building energy consumption. *Renew. Sustain. Energy Rev.* **2012**, *16*, 3586–3592. [CrossRef]
4. Liang, J.; Du, R. Model-based fault detection and diagnosis of HVAC systems using support vector machine method. *Int. J. Refrig.* **2007**, *30*, 1104–1114. [CrossRef]

5. Suganthi, L.; Samuel, A.A. Energy models for demand forecasting—A review. *Renew. Sustain. Energy Rev.* **2012**, *16*, 1223–1240. [CrossRef]
6. Manzano-Agugliaro, F.; Montoya, F.G.; Sabio-Ortega, A.; Garcia-Cruz, A. Review of bioclimatic architecture strategies for achieving thermal comfort. *Renew. Sustain. Energy Rev.* **2015**, *49*, 736–755. [CrossRef]
7. Gallo, C. Bioclimatic architecture. *Renew. Energy* **1994**, *5*, 1021–1027. [CrossRef]
8. Tzikopoulos, A.F.; Karatza, M.C.; Paravantis, J.A. Modeling energy efficiency of bioclimatic buildings. *Energy Build.* **2005**, *37*, 529–544. [CrossRef]
9. Albatici, R.; Passerini, F. Bioclimatic design of buildings considering heating requirements in Italian climatic conditions. A simplified approach. *Build. Environ.* **2011**, *46*, 1624–1631. [CrossRef]
10. Panwar, N.L.; Kaushik, S.C.; Kothari, S. Role of renewable energy sources in environmental protection: A review. *Renew. Sustain. Energy Rev.* **2011**, *15*, 1513–1524. [CrossRef]
11. Hua, Y.; Oliphant, M.; Hu, E.J. Development of renewable energy in Australia and China: A comparison of policies and status. *Renew. Energy* **2016**, *85*, 1044–1051. [CrossRef]
12. Scarlat, N.; Dallemand, J.-F.; Monforti-Ferrario, F.; Banja, M.; Motola, V. Renewable energy policy framework and bioenergy contribution in the European Union—An overview from National Renewable Energy Action Plans and Progress Reports. *Renew. Sustain. Energy Rev.* **2015**, *51*, 969–985. [CrossRef]
13. Ahmad, A.S.; Hassan, M.Y.; Abdullah, M.P.; Rahman, H.A.; Hussin, F.; Abdullah, H.; Saidur, R. A review on applications of ANN and SVM for building electrical energy consumption forecasting. *Renew. Sustain. Energy Rev.* **2014**, *33*, 102–109. [CrossRef]
14. Fumo, N. A review on the basics of building energy estimation. *Renew. Sustain. Energy Rev.* **2014**, *31*, 53–60. [CrossRef]
15. Kalogirou, S.A. Artificial neural networks in energy applications in buildings. *Int. J. Low Carbon Technol.* **2006**, *1*, 201–216. [CrossRef]
16. Foucquier, A.; Robert, S.; Suard, F.; Stephan, L.; Jay, A. State of the art in building modelling and energy performances prediction: A review. *Renew. Sustain. Energy Rev.* **2013**, *23*, 272–288. [CrossRef]
17. Mena, R.; Rodríguez, F.; Castilla, M.; Arahal, M.R. A prediction model based on neural networks for the energy consumption of a bioclimatic building. *Energy Build.* **2014**, *82*, 142–155. [CrossRef]
18. Al-Homoud, M.S. Computer-aided building energy analysis techniques. *Build. Environ.* **2001**, *36*, 421–433. [CrossRef]
19. Wang, S.W.; Xu, X.H. Simplified building model for transient thermal performance estimation using GA-based parameter identification. *Int. J. Therm. Sci.* **2006**, *45*, 419–432. [CrossRef]
20. Lu, X.; Lu, T.; Kibert, C.J.; Viljanen, M. Modeling and forecasting energy consumption for heterogeneous buildings using a physical-statistical approach. *Appl. Energy* **2015**, *144*, 261–275. [CrossRef]
21. Lomet, A.; Suard, F.; Cheze, D. Statistical modeling for real domestic hot water consumption forecasting. *Energy Procedia* **2015**, *70*, 379–387. [CrossRef]
22. Ma, Z.; Li, H.; Sun, Q.; Wang, C.; Yan, A.; Starfelt, F. Statistical analysis of energy consumption patterns on the heat demand of buildings in district heating systems. *Energy Build.* **2014**, *85*, 464–472. [CrossRef]
23. Fumo, N.; Biswas, M.A.R. Regression analysis for prediction of residential energy consumption. *Renew. Sustain. Energy Rev.* **2015**, *47*, 332–343. [CrossRef]
24. Neto, A.H.; Fiorelli, F.A.S. Comparison between detailed model simulation and artificial neural network for forecasting building energy consumption. *Energy Build.* **2008**, *40*, 2169–2176. [CrossRef]
25. Aydinalp-Koksal, M.; Ugursal, V.I. Comparison of neural network, conditional demand analysis, and engineering approaches for modeling end-use energy consumption in the residential sector. *Appl. Energy* **2008**, *85*, 271–296. [CrossRef]
26. Ferreira, P.M.; Ruano, A.E.; Pestana, R.; Kóczy, L.T. Evolving rbf predictive models to forecast the portuguese electricity consumption. *Intell. Control Syst. Signal Process.* **2009**, *2*, 414–419.
27. Li, K.; Su, H.; Chu, J. Forecasting building energy consumption using neural networks and hybrid neuro-fuzzy system: A comparative study. *Energy Build.* **2011**, *43*, 2893–2899. [CrossRef]
28. Karatasou, S.; Santamouris, M.; Geros, V. Modeling and predicting building's energy use with artificial neural networks: Methods and results. *Energy Build.* **2006**, *38*, 949–958. [CrossRef]
29. Kaytez, F.; Taplamacioglu, M.C.; Cam, E.; Hardalac, F. Forecasting electricity consumption: A comparison of regression analysis, neural networks and least squares support vector machines. *Int. J. Electr. Power Energy Syst.* **2015**, *67*, 431–438. [CrossRef]

30. Dong, B.; Cao, C.; Lee, S.E. Applying support vector machines to predict building energy consumption in tropical region. *Energy Build.* **2005**, *37*, 545–553. [CrossRef]
31. Jung, H.C.; Kim, J.S.; Heo, H. Prediction of building energy consumption using an improved real coded genetic algorithm based least squares support vector machine approach. *Energy Build.* **2015**, *90*, 76–84. [CrossRef]
32. Suganthi, L.; Iniyan, S.; Samuel, A.A. Applications of fuzzy logic in renewable energy systems—A review. *Renew. Sustain. Energy Rev.* **2015**, *48*, 585–607. [CrossRef]
33. Ciabattoni, L.; Grisostomi, M.; Ippoliti, G.; Longhi, S. Fuzzy logic home energy consumption modeling for residential photovoltaic plant sizing in the new Italian scenario. *Energy* **2014**, *74*, 359–367. [CrossRef]
34. Li, K.; Su, H. Forecasting building energy consumption with hybrid genetic algorithm-hierarchical adaptive network-based fuzzy inference system. *Energy Build.* **2010**, *42*, 2070–2076. [CrossRef]
35. Hamzacebi, C.; Es, H.A. Forecasting the annual electricity consumption of Turkey using an optimized grey model. *Energy* **2014**, *70*, 165–171. [CrossRef]
36. Lee, Y.-S.; Tong, L.-I. Forecasting energy consumption using a grey model improved by incorporating genetic programming. *Energy Convers. Manag.* **2011**, *52*, 147–152. [CrossRef]
37. Guo, J.J.; Wu, J.Y.; Wang, R.Z. A new approach to energy consumption prediction of domestic heat pump water heater based on grey system theory. *Energy Build.* **2011**, *43*, 1273–1279. [CrossRef]
38. Dagnely, P.; Ruette, T.; Tourwe, T. Predicting hourly energy consumption. Can you beat an autoregressive model? In Proceeding of the 24th Annual Machine Learning Conference of Belgium and the Netherlands, Benelearn, Delft, The Netherlands, 19 June 2015.
39. *Estación Experimental "Las Palmerillas". Datos Meteorológicos. Campañas Agrícolas 76/77–94/95*; Caja Rural de Almería: Almería, Spain, 1997.
40. Castilla, M.Á.; Álvarez, J.D. *Francisco de Asis Berenguel, Manuel. Comfort Control in Buildings*, 1st ed.; Springer London: London, UK, 2014.
41. Heras, M.R.; Jimenez, M.J.; San Isidro, M.J.; Zarzalejo, L.F.; Perez, M. Energetic analysis of a passive solar design, incorporated in a courtyard after refurbishment, using an innovative cover component based in a sawtooth roof concept. *Sol. Energy* **2005**, *78*, 85–96. [CrossRef]
42. Ferreira, P.M.; Ruano, A.E. Evolutionary multiobjective neural network models identification: Evolving task-optimised models. *New Adv. Intell. Signal Process.* **2011**, *372*, 21–53.
43. Ruano, A.E.; Ferreira, P.M.; Fonseca, C.M. An overview of nonlinear identification and control with neural networks. In *Intelligent Control Systems Using Computational Intelligence Techniques*; Ruano, A.E., Ed.; Institution of Electrical Engineers: London, UK, 2005; pp. 37–87.
44. Marquardt, D.W. An algorithm for least-squares estimation of nonlinear parameters. *J. Soc. Ind. Appl. Math.* **1963**, *11*, 431–441. [CrossRef]
45. Hornik, K.; Stinchcombe, M.; White, H. Multilayer feedforward networks are universal approximators. *Neural Netw.* **1989**, *2*, 359–366. [CrossRef]
46. Fraser, A.M.; Swinney, H.L. Independent coordinates for strange attractors from mutual information. *Phys. Rev. A* **1986**, *33*, 1134–1140. [CrossRef] [PubMed]
47. Kennel, M.B.; Brown, R.; Abarbanel, H.D.I. Determining embedding dimension for phase-space reconstruction using a geometrical construction. *Phys. Rev. A* **1992**, *45*, 3403–3411. [CrossRef] [PubMed]
48. Zhou, A.; Qu, B.-Y.; Li, H.; Zhao, S.-Z.; Suganthan, P.N.; Zhang, Q. Multiobjective evolutionary algorithms: A survey of the state of the art. *Swarm Evolut. Comput.* **2011**, *1*, 32–49. [CrossRef]
49. Zitzler, E.; Deb, K.; Thiele, L. Comparison of multiobjective evolutionary algorithms: Empirical results. *Evolut. Comput.* **2000**, *8*, 173–195. [CrossRef] [PubMed]
50. Fonseca, C.M.; Fleming, P.J. An overview of evolutionary algorithms in multiobjective optimization. *Evolut. Comput.* **1995**, *3*, 1–16. [CrossRef]
51. Fonseca, C.M.; Fleming, P.J. Multiobjective optimization and multiple constraint handling with evolutionary algorithms. I. A unified formulation. *IEEE Trans. Syst. Man Cybern. Part A Syst. Hum.* **1998**, *28*, 26–37. [CrossRef]
52. Ruano, A.E.B.; Jones, D.I.; Fleming, P.J. A new formulation of the learning problem for a neural network controller. In Proceeding of the 30th IEEE Conference on Decision and Control, Brighton, UK, 11–13 December 1991; pp. 865–866.

53. Ferreira, P.M.; Faria, E.A.; Ruano, A.E. Neural network models in greenhouse air temperature prediction. *Neurocomputing* **2002**, *43*, 51–75. [CrossRef]
54. Ferreira, P.M.; Ruano, A.E.; Ieee, I. Exploiting the separability of linear and nonlinear parameters in radial basis function networks. In Proceeding of the IEEE 2000 Adaptive Systems for Signal Processing, Communications, and Control Symposium, Lake Louise, AB, Canada, 1–4 October 2000; pp. 321–326.
55. Haykin, S. *Neural Networks: A Comprehensive Foundation*, 2nd ed.; Prentice Hall: Upper Saddle River, NJ, USA, 1999.
56. Ruano, A.; Khosravani, H.R.; Ferreira, P.M. A randomized approximation convex hull algorithm for high dimensions. *IFAC PapersOnLine* **2015**, *48*, 123–128. [CrossRef]